Indian Journal of Chemistry
Vol. 63, September 2024, pp. 875-881
DOI: 10.56042/ijc.v63i9.10838

Electrocatalytic activity of $La_{0.6}Sr_{0.4}Co_{1-y}Cu_yO_3$ (y = 0.1, 0.2, and 0.3) for oxygen evolution in an alkaline medium at 25°C

Basant Lal*[a], Pankaj Chauhan[a] & Anupam Srivastava[b]
[a] Department of Chemistry, Institute of Applied Sciences and Humanities, GLA University, Mathura 281 406, India
[b] Department of Chemistry, Faculty of Science, Dayalbagh Educational Institute Dayalbagh, Agra 282 005, India
E-mail: basant.lal@gla.ac.in

Received 01 May 2024; accepted (revised) 30 August 2024

Binary metal substituted lanthanum cobaltate *viz*., $La_{0.6}Sr_{0.4}Co_{1-y}Cu_yO_3$ (y = 0.1, 0.2, and 0.3) have been prepared by sol-gel method using alginic acid as a precursor and characterized by the TGA, IR, XRD, and SEM techniques. They have also been studied for their electrochemical performance towards the electrocatalytic splitting of water in an alkaline medium. Recorded cyclic voltammetry of the oxide electrodes on nickel support show a pair of oxidation-reduction peaks in the anodic peak potential region (Epa ≈ 508-553 mV) and in the cathodic peak potential region (Epc ≈ 305-322 mV). The polarization curves of each oxide electrode with Tafel slope (b) range from 95 to 101 mV dec^{-1}, and the apparent current density (ja) ranges from 31 to 45 mA cm^{-2} at 0.7 V. Doping of copper in a $La_{0.6}Sr_{0.4}CoO_3$ matrix improves the electrocatalytic activity for the oxygen evolution reaction in an alkaline solution. The observed values of the reaction order with respect to the concentration change of [OH^-] are unity, and the strongly negative value of the reaction entropy indicates that the electrocatalytic oxygen evolution by water splitting occurs by the same mechanism involving the adsorption phenomenon of reaction intermediates on the electrode surface.

Keywords: Electrocatalysis, Cyclic voltammetry, Tafel-polarization, Perovskite-type oxide, Oxygen evolution reaction

The high demand for clean fuels by our growing population is a great challenge for science to solve this problem. Conventional energy resources are limited and their combustion produces large amounts of CO_2 and other pollutants. Researchers are working to develop newer technologies for the economical production of hydrogen by water splitting. Perovskite-type oxide materials play a very important role in the electrocatalysis of water. To split water by the electrolysis method, we have attempted to synthesize perovskite family oxides, namely $La_{0.6}Sr_{0.4}Co_{1-y}CuyO_3$ (y = 0.1, 0.2, and 0.3), by a novel sol-gel route using alginic acid as a precursor. These oxides were found to be more catalytically active than those prepared by other conventional methods[1]. The oxides prepared by the conventional high-temperature ceramic methods for oxygen evolution have low electrochemical surface area and low reduced homogeneity. To improve the electrocatalytic activity, perovskite oxides have been prepared by other methods, such as spray drying[2], co-precipitation[3], freeze-drying[4], microwave-assisted[5], sonochemical reactions[6], sol-gel combustion[7], citrate precursor techniques[8], the hydrothermal method[9] and microemulsion precursors[10]. For oxygen evolution, a very thin oxide layer was deposited on a conductive support obtained by various techniques such as spray pyrolysis[11] and thermal decomposition[12]. New acceptable low-temperature methods using nitrite cyanide and solid hydroxide solutions[13] and organic amorphous methods such as citrate and malic acid as precursors have also been reported in the literature.

Binary substituted lanthanum cobaltates are very useful electrode materials used in various technologically important processes such as the production of O_2, Cl_2, chlorates, O_2 reduction, H_2 evolution, *etc.*[14] Metal substituted perovskite-type oxides are used as catalysts in a variety of reactions including decomposition of H_2O_2[15], production of NH_3 by Haber process[16], energy storage[17], gas sensors[18], electrochemical sensors[19], multilayer chip inducers[20], energy conversion devices[21], clean energy applications[22], *etc.* Due to the use of less expensive metals such as Cu, Co, La, and Sr, the binary substituted oxides, namely $La_{0.6}Sr_{0.4}Co_{1-y}Cu_yO_3$, are considered economical and are the most widely used among the perovskite-type oxide families. These oxides have variable valence, larger surface area and

are non-toxic to human health. The present study is an attempt to minimize the oxygen overpotential by using oxide electrodes of $La_{0.6}Sr_{0.4}Co_{1-y}Cu_yO_3$ (y = 0.1, 0.2 and 0.3) obtained by the novel alginic acid-sol-gel route.

Materials and Methods

$La_{0.6}Sr_{0.4}Co_{1-y}Cu_yO_3$ (y = 0.1, 0.2, and 0.3) was prepared by alginic acid-sol-gel route using strontium nitrate ($Sr(NO_3)_2$; Sigma-Aldrich, 99.9%), lanthanum (III) nitrate hexahydrate ($La(NO_3)_3.6H_2O$; Sigma-Aldrich, 99.9%), copper (II) nitrate trihydrate ($Cu(NO_3)_2.3H_2O$; Sigma-Aldrich, 99%) and cobalt (II) nitrate hexahydrate ($Co(NO_3)_2.6H_2O$; Sigma-Aldrich, 98%). The nitrate salts of each metal were taken in their stoichiometric ratio and dissolved in double distilled water with stirring. The alginic acid solution was prepared with a similar volume of double distilled water and ammonia (NH_3) was added to give a *p*H of 7 for complete dissolution of the alginic acid. Both solutions were stirred separately at room temperature to ensure homogeneity. The resulting homogeneous brown-coloured alginic acid solution was added dropwise to the metal salt solution with continuous stirring until a milky brown solution was formed, and then the gel of the metal-alginic acid composite was converted to a black shiny gel by evaporation at 100°C. The required perovskite-type oxides were produced by thermal decomposition of this combination at 600°C for 5 hours in an electric muffle furnace.

To determine the thermal stability of the gel form, the gel of metal salt with alginic acid precursor was subjected to thermogravimetric analysis (model: Mettler Toledo TGA/DSC 3+) in the temperature range between 25°C and 800°C at constant nitrogen flow. FT-IR Spectroscopy and XRD spectroscopy were used to confirm the formation of a stable perovskite oxide phase. The FT-IR spectrum of the perovskite oxide was recorded between the wavenumber 400 cm^{-1} and 4000 cm^{-1} using IRSPIRIT-T Shimadzu spectrophotometer and that for the XRD powder pattern, Cu-Kα - the radiation source, λ = 1.54059 Å and from 2θ = 20° to 80° was studied. Morphology and crystallite size were observed using a Zeiss scanning electron microscope. For the electrochemical study, the oxide electrode was prepared by repeatedly applying oxide slurry to the nickel plate pretreated on one side in concentrated HCl, rinsed in acetone and washed with double distilled water, and then sintered in an electric furnace at 300°C for 1 hour to obtain the desired oxide loading (~ 5-6 mg cm^{-2}). For electrical contact, a flattened end of a copper wire was connected to the opposite side of the nickel plate with silver paste and attached with epoxy resin (Araldite) to form an exposed oxide area of about 0.5 cm^{-2}. The electrocatalytic properties of the fabricated electrode were carried out in a single chamber pyrex glass cell with a Ni/oxide electrode as the working electrode, a graphite rod as the counter electrode and Hg/HgO/ 1MKOH (0.098V vs. NHE) as the reference electrode using the electrochemical workstation CHI[12].

Results and Discussion

Thermogravimetric analysis (TGA)

The TGA sample was obtained by evaporation of the aqueous solution of the components metal nitrates in stoichiometric ratio together with an appropriate amount of alginic acid at 100°C. The thermogram of the sample (solid mass) was recorded in an inert atmosphere in the temperature range from 25 to 800°C and is shown in Fig. 1. This thermogram shows the three different regions of weight loss. The first transition, which involves weight loss due to the elimination of moisture from the sample, occurs at 110°C. The second transition started at ~200°C and showed a high weight loss due to the decomposition of the carboxylate group by the loss of CO_2 from the metal alginate[23]. The third transition at 600°C showed a low weight loss due to the elimination of N_2 from the nitrates and other organic components.

Fourier-Transform Spectroscopy (FT-IR)

To confirm the formation of the oxide, the sample was analyzed using the FT-IR technique in the

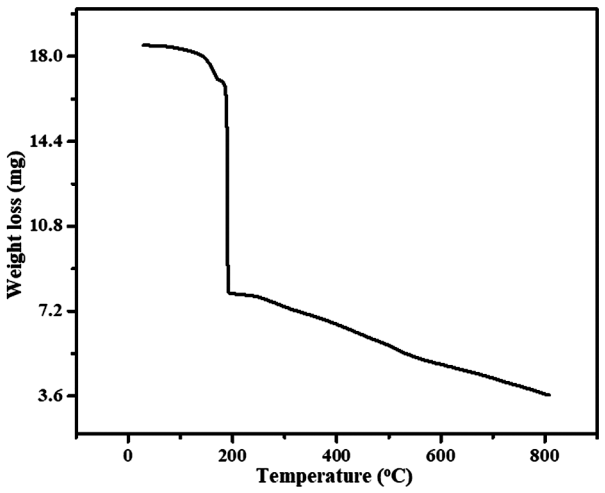

Fig. 1 — TGA of solid mass obtained after evaporation of solution alginic acid and metal salts solution at 100°C.

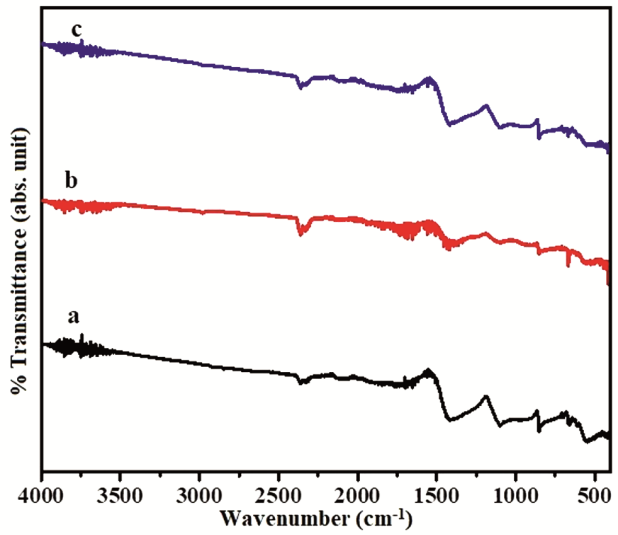

Fig. 2 — FT-IR spectra of (a) $La_{0.6}Sr_{0.4}Co_{0.9}Cu_{0.1}O_3$ (b) $La_{0.6}Sr_{0.4}Co_{0.8}Cu_{0.2}O_3$ (c) $La_{0.6}Sr_{0.4}Co_{0.7}Cu_{0.3}O_3$ prepared at 600°C.

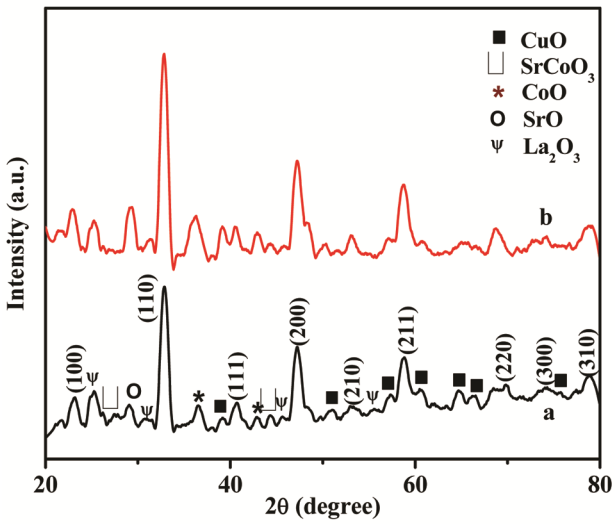

Fig. 3 — XRD spectrum of (a) $La_{0.6}Sr_{0.4}Co_{0.9}Cu_{0.1}O_3$ and (b) $La_{0.6}Sr_{0.4}Co_{0.8}Cu_{0.2}O_3$ prepared at 600°C

wavenumber range between 400-4000 cm^{-1}. The IR spectrum of all Cu– and Sr-substituted lanthanum cobaltite is shown in Fig. 2. Cu-substituted strontium lanthanum cobaltate oxides characteristic peaks in all cases show the absorption bands at 555 cm^{-1}, which are due to the band oscillation mode of $LaCoO_3$. Another band of the absorption peak at 419 cm^{-1} indicates the formation of O–Co–O and La–O–Co, which represents the formation of the crystalline phase structure of $LaCoO_3$[24]. Another vibrational peak at 1427 cm^{-1} corresponds to lanthanum cobaltite[25]. Another peak at 659 cm^{-1} was found in the oxide phase, indicating spinel phase Co_3O_4 along with perovskite oxide due to strontium substitution in perovskite oxide[26]. Some additional peaks were observed in the oxide phase at 851 cm^{-1}, and 3500 cm^{-1}, which are due to the vibration of Sr-O[27] and the stretching vibration of the O–H bond of H_2O[28], and another absorption peak at 2350 cm^{-1} is attributed to the stretching vibration of O=C=O[29], but the peak at 1100 cm^{-1} was not identified in the IR spectrum of the oxides.

X-Ray Diffraction (XRD)

Two representative XRD powder patterns of $La_{0.6}Sr_{0.4}Co_{0.9}Cu_{0.1}O_3$ and $La_{0.6}Sr_{0.4}Co_{0.8}Cu_{0.2}O_3$ are given in Fig. 3. The XRD powder patterns of oxides exhibited many reflection peaks that have a clear agreement with their corresponding peaks as shown in their JCPDS file 48-0121 and confirmed the formation of perovskite phase as a major constituent with (100), (110), (111), (200), (210), (211) (220), (300), and (310) XRD planes. XRD spectra also contain some additional peaks impurity in very fewer quantities such as strontium oxide (SrO) (JCPDS file no. 6- 0520), strontium cobalt oxide ($SrCoO_3$) (JCPDS file no. 49- 0692) cobalt oxide (CoO) (JCPDS file 43-1004), (La_2O_3) (JCPDS file 83-1348) and (CuO) (JCPDS file 45-0937) in both spectra. The crystallite size (S) of oxides was calculated by the Debye Scherrer formula ($S = \frac{0.9 \times \lambda}{\beta \cos \theta}$), where β is full width at half maximum (FWHM), θ is the Bragg angle. The value of crystallite size of strontium-substituted cobaltates $La_{0.6}Sr_{0.4}Co_{0.9}Cu_{0.1}O_3$ and $La_{0.6}Sr_{0.4}Co_{0.8}Cu_{0.2}O_3$ is estimated to be ~16, and ~15 nm, respectively. These values are comparatively lower than that obtained by Singh *et al.*[30] reported for oxides prepared by another sol-gel method.

Scanning Electron Microscopy (SEM)

Surface morphology of the oxide was observed by the SEM analysis and the scanning electron micrographs of $La_{0.6}Sr_{0.4}Co_{0.9}Cu_{0.1}O_3$ at different magnifications are shown in Fig. 4. SE micrographs exhibited agglomerated granules of different nano-sizes (70 -100 nm).

Cyclic voltammetry (CV)

Cyclic voltammograms of fabricated electrodes (oxide/Ni) were recorded at 20 mV sec^{-1} between potential regions 0 to 0.7 V *vs* Hg/HgO in 1M KOH at 25°C and a representative cyclic voltammetric curve of $La_{0.6}Sr_{0.4}Co_{0.8}Cu_{0.2}O_3$ is shown in Fig. 5. From the CV curve, it is clear that there is the formation of a

redox couple ($Ni^{2+} \leftrightarrow Ni^{3+} + e^-$), just before oxygen evolution reactions. The voltammograms exhibited pseudocapacitive in nature with their corresponding values of the anodic, cathodic and formal redox peak potentials E_{pa} 531±23 mV, E_{pc} ≅ 314±9 mV, ΔE_p^o ≅ 217±14 mV [Table 1].

Roughness factor (R_F)

The oxide roughness factor (R_F) of each oxide/1M KOH electrode was determined from the cyclic voltammograms recorded at the different scan rates (10, 20, 40, 60, 80, and 100 mV s^{-1}) in 1 M KOH solution at 25°C between a very narrow potential region 0.075 and 0.125 V which was free from any charge transfer reaction (Fig. 6(a)). The double layer capacitance (C_{dl}) was estimated from the slope of the straight line curve log j *vs* scan rate and shown in Fig. 6(b) and the observed values of C_{dl} are 4586, 2206, and 9418 μF for the $La_{0.6}Sr_{0.4}Co_{0.9}Cu_{0.1}O_3$, $La_{0.6}Sr_{0.4}Co_{0.8}Cu_{0.2}O_3$, and $La_{0.6}Sr_{0.4}Co_{0.7}Cu_{0.3}O_3$, respectively. The roughness factor for each electrode was calculated from the C_{dl} values by considering the C_{dl} of smooth oxide surface is 60 μF[30] and given in Table 2. The calculated value of R_F was observed to be almost similar for each oxide electrode. However, 0.3 mol Cu-doped strontium lanthanum cobaltate showed a considerably higher value of R_F (~157) and also showed the most active

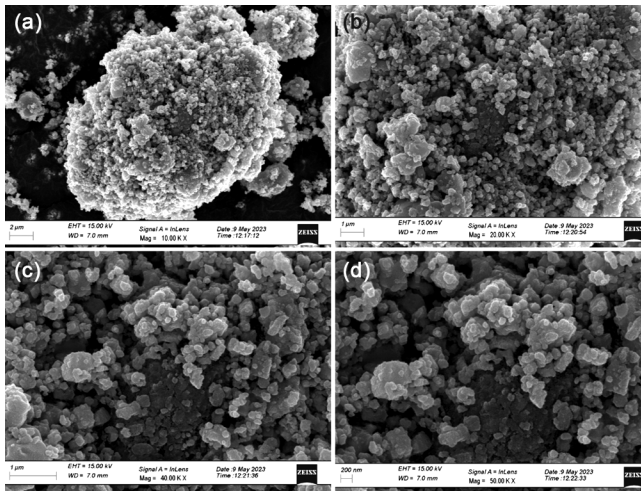

Fig. 4 — SE micrographs of $La_{0.6}Sr_{0.4}Co_{0.9}Cu_{0.1}O_3$ at different magnifications: (a) 10000X (b) 20000X (c) 40000X and (d) 50000X

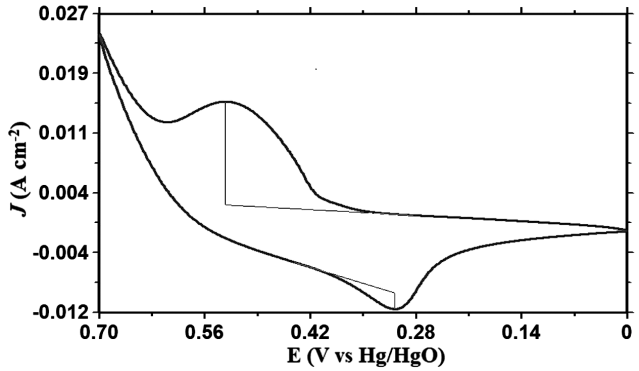

Fig. 5 — CV curve of Ni/$La_{0.6}Sr_{0.4}Co_{0.8}Cu_{0.2}O_3$ electrode at 20 mV s^{-1} in 1M KOH at 25°C recorded between 0 to 0.7 V

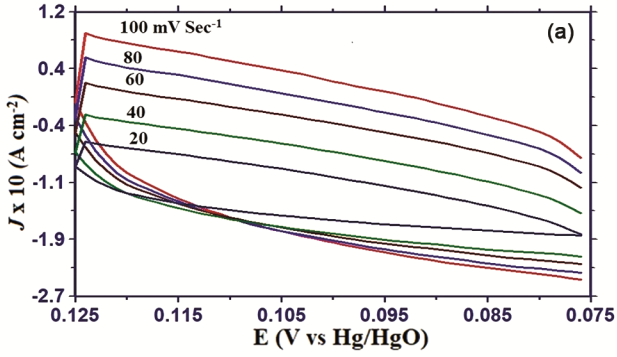

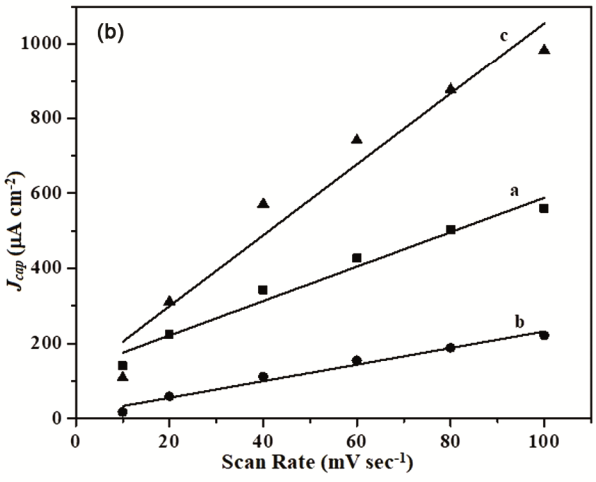

Fig. 6(a) — CV curves of Ni/ $La_{0.6}Sr_{0.4}Co_{0.8}Cu_{0.2}O_3$ electrode at different scan rates in 1 M KOH at 25°C recorded between 0.075 to 0.125 V

Table 1 — Cyclic voltammetric data of oxide/Ni electrodes for OER in 1M KOH at 25°C

Oxides	E_{pa}, mV	E_{pc}, mV	ΔE_p, mV	ΔE_p^o, mV
$La_{0.6}Sr_{0.4}Co_{0.9}Cu_{0.1}O_3$	532	309	223	421
$La_{0.6}Sr_{0.4}Co_{0.8}Cu_{0.2}O_3$	508	305	203	407
$La_{0.6}Sr_{0.4}Co_{0.7}Cu_{0.3}O_3$	553	322	231	438

Table 2 — Kinetic parameters for O_2 evolution on Ni/oxide electrodes in 1M KOH (25°C)

Oxide	Tafel slope, mV/decade^{-1}	E, mV at j = 10 mA/cm^{-2}	J, mA/cm^{-2} at E = 750 mV		C_{dl}, µF	R_F
			j_{app}	j_{tr}		
$La_{0.6}Sr_{0.4}Co_{0.9}Cu_{0.1}O_3$	95	658	31.09	0.409	4586	76
$La_{0.6}Sr_{0.4}Co_{0.8}Cu_{0.2}O_3$	101	657	35.82	0.995	2206	36
$La_{0.6}Sr_{0.4}Co_{0.7}Cu_{0.3}O_3$	96	643	45.42	0.289	9418	157

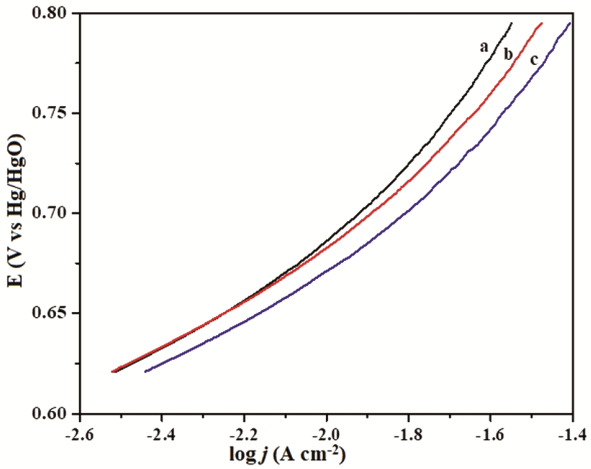

Fig. 7 — Tafel polarization curves on Ni/oxide electrodes at 25°C in 1M KOH: (a) $La_{0.6}Sr_{0.4}Co_{0.9}Cu_{0.1}O_3$ (b) $La_{0.6}Sr_{0.4}Co_{0.8}Cu_{0.2}O_3$ and (c) $La_{0.6}Sr_{0.4}Co_{0.7}Cu_{0.3}O_3$

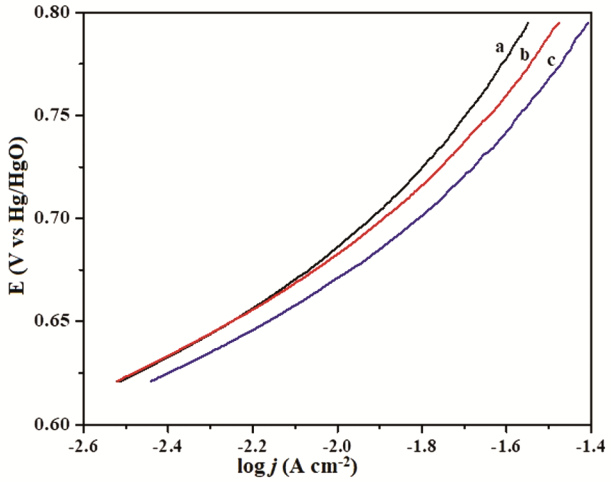

Fig. 8 — A typical plot of log j (at E = 0.7 V) *vs* log [OH^-] for $La_{0.6}Sr_{0.4}Co_{0.9}Cu_{0.1}O_3$ electrode

electrode from an O_2 evolution standpoint. The strontium doping in the lanthanum cobaltate matrix prepared by the malic acid sol-gel route significantly improved in R_F-value was observed by Singh *et al.*[30]

Electrocatalytic activity

The electrocatalytic activity of fabricated oxide electrodes on Ni for oxygen evolution was measured at a scan rate of 0.2 mVsec^{-1} by the Tafel polarization technique in 1M KOH at 25°C and shown in Fig. 7 and observed electrode kinetic data are given in Table 2. The observed values of the Tafel slopes range from 95 to 101 mV dec^{-1}. The Cu-substitution in the $La_{0.6}Sr_{0.4}CoO_3$ matrix marginally reduces the Tafel slope value, and the greater reduction in the Tafel slope was found for $La_{0.6}Sr_{0.4}Co_{0.9}Cu_{0.1}O_3$ electrode. Table 2 shows that Cu-substitution in the oxide matrix significantly improve the electrocatalytic activity that are mainly apparent from the current density (j_{app}) for OER and the highest values recorded in the case of $La_{0.6}Sr_{0.4}Co_{0.7}Cu_{0.3}O_3$. It is considered as the most active electrode for OER among all electrodes studied in the present investigation and have the highest value of apparent current density, 45.4 mA cm^{-2} at 0.75 V. Increase in electrocatalytic activity is most probably due to increase in oxygen vacancy in the prepared oxide and reduction in the vacancy at La and Co sites which enhances the number of oxygen vacancies. The prepared oxide electrodes showed similar catalytic activity as observed by Singh *et al.*[31]

Order of reaction

The order of oxygen evolution reaction was determined from the Tafel polarization curves recorded at different concentrations of KOH (0.25, 0.5, 0.75, 1.0, and 1.5 M) keeping ionic strength of medium (µ = 1.5) constant with KNO_3 as an inert electrolyte at 25°C. The order of reaction was estimated from the slope of log j *vs* log [OH^-] plot at constant potential (0.7V). A representative plot of log j *vs* log [OH^-] for the $La_{0.6}Sr_{0.4}Co_{0.9}Cu_{0.1}O_3$ electrode is given in Fig. 8. The order of reaction for each oxide electrode was found to be approximately unity (~1) which indicated that the electrochemical formation of oxygen on the electrode/solution interface follows a similar mechanism as reported elsewhere[30-32].

Activation energy

The thermodynamic parameters such as apparent electrochemical activation energy ($\Delta H_c^{0\neq}$) at constant

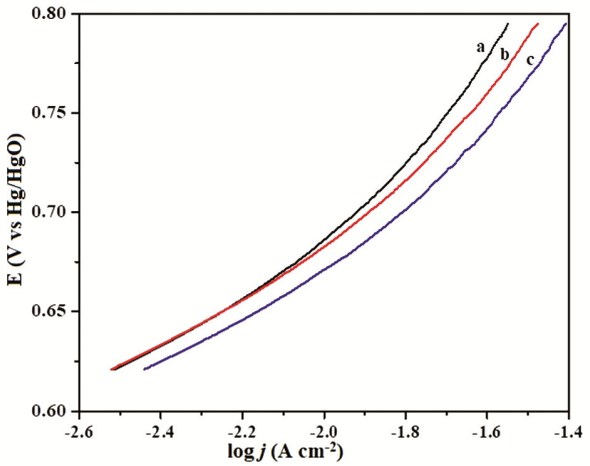

Fig. 9 — The Arrhenius plot at 0.7 V in 1M KOH for $La_{0.6}Sr_{0.4}Co_{0.9}Cu_{0.1}O_3$

reversible potential, standard electrochemical activation energy ($\Delta H_{el}^{0\neq}$) at constant applied potential (at 0.7V), and entropy of reaction ($\Delta S_{el}^{0\neq}$) on fabricated $La_{0.6}Sr_{0.4}Co_{0.9}Cu_{0.1}O_3$ electrode for OER were determined from the Tafel polarization curves recorded at different temperatures in 1M KOH solution. The value of $\Delta H_{el}^{0\neq}$ was estimated from the slope of Arrhenius plot log j *vs* 1/T shown in Fig. 9. The calculated value of $\Delta H_{el}^{0\neq}$ was 16.2 kJ mol^{-1} and $\Delta S_{el}^{0\neq} = 2.303\ R\ [\Delta H_{el}^{0\neq}/2.303RT + \log j - \log nF\omega C_{OH^-}]$ equation was used for the calculation of their entropy of reaction –263 J deg^{-1} mol^{-1}. This highly negative value entropy of reaction indicates the mechanism of the electrochemical oxygen evolution involved in the adsorption of the reaction intermediate[32].

Conclusions

The present investigation includes the preparation of Cu and Sr-substituted lanthanum cobaltate by alginic acid sol-gel route and physicochemically characterized by the TGA, IR, XRD, and SEM analyses. XRD spectra of oxide showed the formation of perovskite as a major phase along with some additional phases in trace amounts. Based on the results of the present investigation it is recommended that the sol-gel method could be useful for the economical formation of highly active electrocatalysts for oxygen evolution reaction in alkaline medium. Copper substitution at the cobalt site in $La_{0.6}Sr_{0.4}CoO_3$ improved electrocatalytic activity for oxygen evolution reaction. Cu-substituted oxide catalysts prepared by alginic acid could play an important role in electrocatalytic applications and energy storage devices.

Acknowledgements

One of the authors B. Lal is thankful to the UPCST for the financial support through a research project (CST/CHEM/D-1120 ID-1167) and also expresses his thanks to Prof. Kamal Shah Institute of Pharmaceutical Research, GLA University Mathura for FT-IR analyses of the oxide samples.

References

1 Sullivan EJMO, Calvo EJ. Comprehensive Chemical Kinetics. 27 (Electrode Kinetic Reaction) R.G. Compton (Ed.) Elsevier Amsterdam, 1987 248 -294.
2 Rivas M B, Fagnard J F, Vanderbemden P, Traianidis M, Henrist C, Cloots R & Vertruyen B, *J Phys Chem Solids*, 72 (2011) 158.
3 Maulana M I & Nandiyanto A B D, *Int J Adv Smart Convergence*, 1 (2019) 7.
4 Alvarez-Galvan C, Trunschke A, Falcon H, Sanchez-Sanchez M, Campos-Martin J M, Schlögl R & Fierro J L G. *Front Energy Res*, 6 (2018) 18.
5 Galal A, Atta N F & Ali S M, *Electrochim Acta*, 56 (2011) 5722.
6 Mehdizadeh P, Masjedi-Arani M, Amiri O, Al-Nayili A & Salavati-Niasari M, *Nanocom Fuel*, 311 (2022) 122544.
7 Samat A A, Somalu M R, Muchtar A & Osman N, *Malaysian J Anal Sci*, 20 (2016) 1458.
8 Popa M & Calderon-Moreno J M, *J Eur Ceram Soc,* 29 (2009) 2281.
9 Nikam S K, Dharmadhikari D V & Athawale A A, Proceedings of the 2nd International Conference on Advanced Nanomaterials and Nanotechnology. 2011, Dec 8–10. Guwahati, India 2013; 33-40. https://doi.org/10.1007/978-3-642-34216-5 3.
10 Meng F, Sun C, Shi J, Zhang H, Xu B & Ding Y, *Int J Hyd Ene,* 44 (2019) 1122.
11 Qi X, Lin Y S & Swartz S L, *Ind Eng Chem Res*, 39 (2000) 646.
12 Singh R N, Bahadur L, Pandey J P, Singh S P, Chartier P & Poillerat G, *J Appl Electrochem*, 24 (1994) 149.
13 Vidyasagar K, Gopalakrishnan J & Rao C N R, *J. Solid State Chem*, 58 (1985) 29.
14 Karimi-Nazarabad M, Ahmadzadeh H & Goharshadi E K, *J Sol Energy Eng*, 227 (2021) 426.
15 Papa F, Berger D, Dobrescu G, State R & Ionescu N I, *Rev Roum Chim*, 63 (2018) 447.
16 Radhakrishnan M, Padmanathan N, Muthu SE, Sivaprakash P& Kadiresan M, *Mater Sci Eng B Solid State Mater Adv Technol,* 284 (2022) 115875.
17 Hussain S, Javed MS, Ullah N, Shaheen A, Aslam N, Ashraf I, Abbas Y, Wang M& Liu G Qiao G, *Ceram Int*, 45 (2019) 15164.
18 Chumakova V T, Marikutsa A V& Rumyantseva M N, *Russ. J Appl Chem*, 94 (2021) 1651.
19 Suvina V, Kokulnathan T, Wang T J & Balakrishna R G, *Mikrochim Acta*, 187 (2020) 1.
20 Lu Y C, Li Y X, Peng R, Chen D M, Yang Q H & Zhang S J, *Mat Sci Forum*, 1027 (2021) 3.
21 Park J S & Kim Y B, *Thin Solid Films*, 599 (2016) 174.
22 Zhu Z, Shi Y & Aruta Y C N, *ACS Appl Energy Mater*, 1 (2018) 5308.

23 Soares J P, Santos J E, Chierice G O & Cavalherio E T G, *Ecle´tica Qu´mica,* 29 (2004) 53.
24 Sun M, Jiang Y, Li F, Xia M, Xue B & Liu D, *Metall Mat Trans*, 51 (2010) 2208.
25 Sarker A R, *J Mater Sci,* 4 (2015) 159.
26 Zhou C, Feng Z, Zhang Y, Hu L, Chen R, Shan B, Yin H, Wang WG & Huang A, *RSC Adv*, 5 (2015) 28054.
27 Alhokbany N, Almotairi S, Ahmed J, Al-Saeedi SI, Ahamad T & Alshehri S M, *J King Saud Univ Sci*, 33 (2021) 101419.
28 Pecchi G, Campos C, Jiliberto MG, Moreno Y & Peña O, *J Mater Sci*, 43 (2008) 5282.
29 Irshad M, Idrees R, Siraj K, Shakir I, Rafique M, Ain Q & Raza R, *Int J Hydrog Energy,* 46 (2021) 10448.
30 Singh N K, Tiwari S K & Singh R N, *Int J Hyd Ene*, 23 (1998) 775.
31 Singh R N & Lal B, *Ind J Chem*, 40A (2010) 1037.
32 Lal B, Raghunandan M K, Gupta M & Singh R N, *Int J Hyd Ene*, 30 (2005) 723.